Eur. Phys. J. B **26**, 241–252 (2002)
DOI: 10.1140/epjb/e20020086

THE EUROPEAN PHYSICAL JOURNAL B
EDP Sciences

Electronic properties of model quantum-dot structures in zero and finite magnetic fields

H. Saarikoski[a], E. Räsänen, S. Siljamäki, A. Harju, M.J. Puska, and R.M. Nieminen

Laboratory of Physics, Helsinki University of Technology, PO Box 1100, 02015 HUT, Finland

Received 16 October 2001 and Received in final form 17 January 2002

Abstract. We have computed electronic structures and total energies of circularly confined two-dimensional quantum dots and their lateral dimers in zero and finite uniform external magnetic fields using different theoretical schemes: the spin-density-functional theory (SDFT), the current-and-spin-density-functional theory (CSDFT), and the variational quantum Monte Carlo (VMC) method. The SDFT and CSDFT calculations employ a recently-developed, symmetry-unrestricted real-space algorithm allowing solutions which break the spin symmetry. Results obtained for a six-electron dot in the weak confinement limit and in zero magnetic field as well as in a moderate confinement and in finite magnetic fields enable us to draw conclusions about the reliability of the more approximative SDFT and CSDFT schemes in comparison with the VMC method. The same is true for results obtained for the two-electron quantum dot dimer as a function of inter-dot distance. The structure and role of the symmetry-breaking solutions appearing in the SDFT and CSDFT calculations for the above systems are discussed.

PACS. 71. Electronic structure of bulk materials – 73.21.-b Electron states and collective excitations in multilayers, quantum wells, mesoscopic, and nanoscale systems – 85.35.Be Quantum well devices (quantum dots, quantum wires, etc.)

1 Introduction

Quantum dots (QD) are man-made solid-state nanoscale structures. As they show typical atomic properties they are often referred to as artificial atoms [1]. The wavefunctions, shell structure and the energy levels are usually reminiscent of real atomic systems. Hund's rules are often obeyed and at certain electron numbers the quantum dots have increased stability corresponding to closed-shell noble gas atoms.

Unlike for normal atoms, a wide variety of geometries is possible by choosing appropriate materials and external confinement: one-dimensional rods, two-dimensional pancakes or three-dimensional spheres. Asymmetric potentials such as ellipsoidal are possible and even quantum dot molecules can be realized by combining two or more quantum dots lying near each other. The versatile physics of the quantum dot systems creates a promising field of potential applications. The field effect transistors in computers could be replaced by quantum-dot logic gates [2]. A double quantum dot 'hydrogen' molecule has been proposed for a basic elementary gate in quantum computers [3]. In this component the electron spins are entangled and serve as a qubit.

In this paper we concentrate on quantum dots realized in a two-dimensional (2D) electron gas at the interface of a GaAs/AlGaAs semiconductor heterostructure. Electrons in this region are confined by an external potential which is usually assumed to be parabolic and their motion is described by the effective-mass theory. The characteristic energy and length scales are such that the electron-electron interaction and the effect of the external magnetic field have comparable energies. Therefore changes in the electronic structure caused by magnetic interactions can happen at magnetic fields of the order of a few teslas, only, *i.e.* at fields attainable in laboratory environment.

Since QD's are nanoscale systems quantum mechanics is required for their accurate description. However, the electronic structure of these systems is very hard or even impossible to solve exactly even in the case of a few electrons, and approximations must be used. Perhaps the most widely used scheme in computational condensed matter physics is the density functional theory (DFT) [4,5]. The method uses the electron density as the basic variable and the ground state properties depend only on this quantity. The exchange and correlation effects between electrons are often approximated by the local density approximation (LDA). The DFT has been generalized to systems of non-zero spin polarization in the spin density functional theory (SDFT) [6]. The DFT and the SDFT formulations ignore the presence of currents induced by external magnetic field or spin polarization. Vignale and Rasolt introduced the current-and-spin-density functional theory (CSDFT) [7], which is a self-consistent extension of the SDFT

[a] e-mail: hri@hugo.hut.fi

to arbitrarily strong magnetic fields for the non-relativistic Pauli Hamiltonian. Therefore it is ideally suited for the electronic structure calculations of QD's in external strong magnetic fields. The variational quantum Monte Carlo (VMC) [8] method is another efficient method to solve the electronic structure of a system of interacting electrons. Its starts from analytic wave functions, the parameters of which are optimized by using the variational principle and random points in the evaluation of integrals.

Our main aim in this work is to study the reliability of the SDFT and CSDFT schemes by comparing their total energies with the corresponding VMC results. The CSDFT reduces to the SDFT scheme when the effects of the induced currents are ignored. The use of the SDFT instead of the CSDFT is tempting, because it simplifies the formalism and calculations [9]. Our results enlighten when this substition is justified and what are its consequences. We consider two systems in our calculations: a single quantum dot with six electrons in an external parabolic circular potential, and a lateral quantum dot 'hydrogen'-like molecule comprising of two dot centra and two electrons. Several authors have calculated properties of the six-electron single dot system in zero [10–14] and finite magnetic [15,16] fields using different schemes. Therefore it serves as a good benchmark test. The two-electron quantum dot molecule has been considered by Wensauer *et al.* using the SDFT [17] in zero field and by G. Burkard *et al.* [18] in zero and finite magnetic fields using the Heitler-London approximation and the Hund-Mulliken molecular-orbital approach.

Our studies are directed towards three different regimes. (i) In the case of the six-electron quantum dot in zero magnetic field we consider the limit when the parabolic confinement potential vanishes. (ii) Moreover, in the case of the six-electron quantum dot with a finite confinement, corresponding to typical experimental situations, we perform calculations as a function of increasing external magnetic field. (iii) Finally, the results for the quantum dot molecule are obtained as a function of the inter-dot separation. The common feature for these three systems is that single-particle energy levels approach each other so that the electron-electron correlation overcomes the effect of the kinetic energy in importance. For the SDFT and CSDFT the result is the breaking of the spin symmetry. This means that, although the external confinement potential is the same for the spin-up and spin-down electrons, the corresponding effective potentials including the electron-electron interactions are different. The ensuing spin-densities are then different, and *e.g.*, in the case of a circular dot the total electron density is not circular. This kind of spin density waves was considered during the advent of the SDFT as a desired flexibility of the theory [6], but their more recent appearance in the context of electronic structures of quantum dots has raised discussion about their interpretation [19–23]. In order to allow the symmetry breaking in our SDFT and CSDFT calculations, we have applied in the calculations a recently developed symmetry-unrestricted real space approach [24]. The testing of this implementation is also one of our goals.

The outline of the paper is the following: in Section 2 we first briefly describe the underlying many-body physics of the systems under consideration. Then we present the basic ideas of the CSDFT, SDFT, and VMC approaches. Computational methods including the real-space Schrödinger equation solver are described in Section 3. The results for the single dot system and the double dot system can be found in Sections 5 and 6, respectively. The results are summarized in Section 7. In this paper the unit of length is the reduced Bohr radius $a_0^* = \hbar^2\epsilon/m^*e^2$. In the case of GaAs the dielectric constant $\epsilon = 12.4$ and the effective mass $m^* = 0.067m_e$ so that $a_0^* \approx 9.79$ nm.

2 Formalisms

2.1 The model Hamiltonian

Throughout the paper we consider vertical quantum dots made in the planar heterostructure of $GaAs/Al_xGa_{1-x}As$. The electron density has a sharp peak in the interface region giving rise to the so-called quasi-two-dimensional electron gas (2DEG). Since the confining potential perpendicular to this conducting layer is strong compared to the confining potential parallel to the plane, we consider the system to be essentially two dimensional, *i.e.* the electron density $n(x, y, z) = n(x, y)\delta(z)$, where z is normal to the plane of interface. We use the effective-mass theory to describe electrons moving in the lattice of the Ga and As atoms.

The Hamiltonian for the system of N electrons moving in the external potential and magnetic field which is applied perpendicular to the plane of the 2DEG (in the z-direction) is

$$H = \frac{1}{2m^*}\sum_{i=1}^{N}\left[-\mathrm{i}\hbar\nabla_i + \mathbf{A_{ext}}(\mathbf{r_i})\right]^2 + \frac{1}{2}\sum_{i\neq j}\frac{e^2}{|\mathbf{r}_i - \mathbf{r}_j|} + \sum_{i=1}^{N} V_\sigma(\mathbf{r_i}), \quad (1)$$

where the spin index $\sigma = \uparrow, \downarrow$. $\mathbf{A_{ext}} = \frac{1}{2}B(y\mathbf{u}_x - x\mathbf{u}_y)$ is the vector potential of the external magnetic field B. The spin-dependent scalar potential consists of a spin-independent external potential V_{ext} and the Zeeman energy,

$$V_\sigma(\mathbf{r_i}) = V_{ext}(\mathbf{r_i}) + g^*\mu_B B s_{z,i}, \quad (2)$$

where g^* is the effective gyromagnetic ratio (reduced Landé g-factor), which has the value of -0.44 for GaAs [25]. μ_B is the Bohr magneton and $s_{z,i} = \pm\frac{1}{2}$ for $\sigma = \uparrow, \downarrow$, respectively.

The wavefunction of the system is $2N$-dimensional so that the many-body problem becomes computationally too difficult and time consuming to solve exactly even in the case of just a few electrons. Therefore we need to make approximations to make the problem computationally feasible for the present day computers.

2.2 Spin-density-functional and current-and-spin-density-functional theories

In the current-and-spin-density-functional theory (CSDFT) by Vignale and Rasolt [7] the Hamiltonian (1) leads to a set of generalized Kohn-Sham equations which have to be solved self-consistently. They include the one-particle Schrödinger equation

$$\left[\frac{\mathbf{p}^2}{2m^*} + \frac{e}{2m^*}\left(\mathbf{p}\cdot(\mathbf{A}_{\rm ext}+\mathbf{A}_{\rm xc}) + (\mathbf{A}_{\rm ext}+\mathbf{A}_{\rm xc})\cdot\mathbf{p}\right) + V_\sigma(\mathbf{r})\right]\psi_{i,\sigma} = \epsilon_{i,\sigma}\psi_{i,\sigma}, \quad (3)$$

where $\mathbf{p} = -\mathrm{i}\hbar\nabla$, $\mathbf{A}_{\rm ext}(\mathbf{r})$ is the vector potential corresponding to the external magnetic field in the z-direction, and $\mathbf{A}_{\rm xc}$ is the so-called exchange-correlation vector potential. The scalar potential V_σ is calculated as

$$V_\sigma(\mathbf{r}) = \frac{e^2}{2m^*c^2}(\mathbf{A}_{\rm ext}+\mathbf{A}_{\rm xc})^2 + V_{\rm ext}(\mathbf{r}) + V_{\rm Hartree}(\mathbf{r}) + V_{\rm Zeeman} + V_{{\rm xc},\sigma}(\mathbf{r}), \quad (4)$$

where $V_{{\rm xc},\sigma}$ is the exchange-correlation scalar potential. The Hartree potential reads as

$$V_{\rm Hartree}(\mathbf{r}) = e\int \frac{n(\mathbf{r}')}{|\mathbf{r}-\mathbf{r}'|}\mathrm{d}\mathbf{r}', \quad (5)$$

where $n(\mathbf{r}) = n_\uparrow(\mathbf{r}) + n_\downarrow(\mathbf{r})$ is the total electron density. The Zeeman potential is just a constant, $V_{\rm Zeeman} = g^*\mu_B B s_{z,i}$. Both the vector and scalar exchange-correlation potentials depend on the spin n_σ and paramagnetic current $\mathbf{j}_{{\rm p},\sigma}$ densities. They are obtained from the one-particle wavefunctions as

$$n_\sigma(\mathbf{r}) = \sum_i |\psi_{i,\sigma}(\mathbf{r})|^2, \quad (6)$$

$$\mathbf{j}_{{\rm p},\sigma} = -\frac{\mathrm{i}\hbar}{2m^*}\sum_i\left[\psi^*_{i,\sigma}\nabla\psi_{i,\sigma} - \psi_{i,\sigma}\nabla\psi^*_{i,\sigma}\right] \quad (7)$$

where the summations are over occupied states.

The total energy of the system with given n_σ and $\mathbf{j}_{{\rm p},\sigma}$ is obtained from the functional

$$E_{\rm tot}[n_\sigma,\mathbf{j}_{{\rm p},\sigma}] = \sum_{i,\sigma}\epsilon_{i,\sigma} - \frac{e^2}{2}\int\int\frac{n(\mathbf{r})n(\mathbf{r}')}{|\mathbf{r}-\mathbf{r}'|}\mathrm{d}\mathbf{r}\mathrm{d}\mathbf{r}' \quad (8)$$
$$-\sum_\sigma\int n_\sigma(\mathbf{r})V_{{\rm xc},\sigma}(\mathbf{r})\mathrm{d}\mathbf{r}$$
$$-\frac{e}{c}\sum_\sigma\int\mathbf{j}_{{\rm p},\sigma}(\mathbf{r})\cdot\mathbf{A}_{{\rm xc},\sigma}(\mathbf{r})\mathrm{d}\mathbf{r} + E_{\rm xc}[n_\sigma,\mathbf{j}_{{\rm p},\sigma}].$$

Following Vignale and Rasolt [7] we obtain the scalar and vector exchange-correlation potentials $V_{{\rm xc},\sigma}$ and $\mathbf{A}_{\rm xc}$ as functional derivatives of the exchange-correlation energy with respect to the spin and current densities, respectively. In the scheme the exchange-correlation energy of the uniform 2DEG per electron in uniform magnetic $\mathbf{B}$ is needed. This is obtained from the $\mathbf{B}=0$ results by Tanatar and Ceperley [26] and from the $\mathbf{B}=\infty$ results by Levesque, Weis and MacDonald [27] using the interpolation form by Ferconi and Vignale [28]. The correlation energy for intermediate spin polarizations is obtained by interpolating between the results for the spin-compensated and totally spin-polarized gases as in the work by Koskinen *et al.* [19]. Numerical instabilities in determining $\mathbf{A}_{\rm xc}$ are avoided by the convolution form introduced by Koskinen *et al.* in a more recent work [29].

The effect of currents on the exchange-correlation energy is due to distortion of the wave function. If the effect of currents can be assumed small the exchange-correlation vector potential $\mathbf{A}_{\rm xc}$ can be neglected and the Kohn-Sham equations of the CSDFT are reduced to the SDFT Kohn-Sham equations. Especially, the one-particle Schödinger equation reads then as

$$\left\{\frac{1}{2m^*}\left[\mathbf{p}+\frac{e}{c}\mathbf{A}_{\rm ext}(\mathbf{r})\right]^2 + \sum_\sigma V_\sigma(\mathbf{r})\right\}\psi_{i,\sigma} = \epsilon_{i,\sigma}\psi_{i,\sigma}, \quad (9)$$

where the scalar potential

$$V_\sigma(\mathbf{r}) = V_{\rm ext}(\mathbf{r}) + V_{\rm Hartree}(\mathbf{r}) + V_{\rm Zeeman} + V_{{\rm xc},\sigma}(\mathbf{r}). \quad (10)$$

Above, the exchange-correlation potential $V_{{\rm xc},\sigma}$ depends now on the spin densities, only. The CSDFT formalism, explained above, reduces to the local spin density approximation (LSDA). Further, if the spin densities are assumed equal, $n_\uparrow = n_\downarrow$, the SDFT-LSDA formalism reduces to the density functional theory (DFT) within the local density approximation (LDA).

According to a theorem by Gunnarsson and Lundqvist [6] the ground-state energy of each specified angular momentum and spin symmetry can be found in the density-functional formalism. The exchange-correlation functional $E_{\rm xc}$ in this theorem, however, should depend on the symmetry of the problem. In the absence of a recipe how to choose this $E_{\rm xc}$ in the actual calculations we have chosen to use the uniform electron-gas data for $E_{\rm xc}$. Due to the LSDA-type local approximations we can specify only the the quantum number S_z of the z-component of the total spin but not the quantum number S of the total spin from the occupation numbers of the eigenstates. In the calculations, we enter S_z explicitly by occupying the $N_\uparrow = N/2 + S_z$ and $N_\downarrow = N/2 - S_z$ lowest spin-up and spin-down eigenstates, respectively. The quantum number L_z of the z-component of the total angular momentum can then be calculated from the angular momenta numerically determined for the occupied states. According to Hirose and Wingreen [21] this procedure may result in a state which is a mixture of several eigenstates corresponding to different S and L quantum numbers and the resulting spin densities break the rotational symmetry of the problem.

3 Computational methods

The Kohn-Sham equations in the SDFT and CSDFT are solved self-consistently. In the SDFT we first insert an initial guess for the scalar potential and solve for the single-particle Schrödinger equation. In the CSDFT an initial guess for the exchange-correlation vector potential must also be provided. We have used the bare external potentials $V_{\rm ext}$ and $\mathbf{A}_{\rm ext}$ to initiate the iterations. Then we compute the new potential using the wavefunctions of the occupied states and solve the Schrödinger equation again using this new potential. This procedure is repeated until the potentials and the wavefunctions have converged. In order to stabilize the iteration process towards self-consistency we have mixed the new potential calculated after solving the electronic structure with the input potential of the iteration and also with that of the previous iteration using the scheme by Koskinen *et al.* [29]. The mixed potential is then used as the input potential for the next iteration. In order to avoid covergence difficulties due to nearly degenerate states close to the Fermi level we occupy in equations (6, 7) the one-particle states according to the Fermi-Dirac distribution corresponding to a finite temperature. The temperature is lowered but kept finite towards the end of the iteration to obtain a good approximation for the ground-state energy.

The one-particle states are solved from the Schrödinger equation (9) in real space using a recently developed multigrid method [24]. The values of the different functions are presented using two-dimensional point grids. The partial differential equations are discretized using central finite differences. The real-space solver uses the Rayleigh quotient multigrid method (RQMG), which is applied directly to the minimization of the Rayleigh quotient of the type $\langle\psi|H|\psi\rangle/\langle\psi|B|\psi\rangle$ on the *finest* grid of the multigrid method. RQMG was originally developed to find the lowest eigenenergy and the ensuing eigenfunction [30], but the method has been extended to the simultaneous solution of several lowest eigenstates [24]. The main idea of the multigrid approach is to use simple relaxation methods, such as the Gauss-Seidel method, in grids of fine and coarse spacing to eliminate the high and low-frequency spatial oscillations of the error, respectively. A converged solution can be obtained usually in a fraction of the iterations normally needed for basic relaxation schemes employing only the finest grid.

In our calculations we usually solve all the states below the Fermi level and a few states above the Fermi level. This allows the finite temperature to be applied to the system and stabilizes also the multigrid solution itself for the occupied states [24]. Compared to the traditional plane-wave solvers the advantage of using a real-space solver is that periodic boundary conditions are not necessary and that the grids can be refined in the regions where greater accuracy is needed. Moreover the real-space methods are more suitable for parallel computing by using domain decomposition.

The Hartree energy is solved in our calculations by approximating the integrals in equation (8) by a sum over all the grid points (i, j)

$$\int\int \frac{n(\mathbf{r})n(\mathbf{r}')}{|\mathbf{r}-\mathbf{r}'|}\mathrm{d}\mathbf{r}\mathrm{d}\mathbf{r}' \approx \sum_{i,j}\sum_{i'\neq i,j'\neq j}\frac{n(i,j)n(i',j')}{|\mathbf{r}(i,j)-\mathbf{r}(i',j')|}h^4 + \sum_{i,j}\frac{2\pi h^3 n^2(i,j)}{\sqrt{\pi}} \quad (11)$$

where h is the grid spacing and the divergence of the integral as $|\mathbf{r}-\mathbf{r}'| \to 0$ is avoided by adding an on-site term, *i.e.* the last term above. The on-site term is obtained by an explicit approximative integration over a uniformly charged disk centered at the gridpoints. The radius of the disk is $h/\sqrt{\pi}$ and the electron density on the disk is $n(i, j)$. The on-site term adds to the accuracy of the numerical integration. If the number of gridpoints is not excessively large, the procedure for the Hartree energy (and potential) is simple and fast in comparison with the total computational work, spent mainly in the solution of the one-particle Schrödinger equation with the multigrid method. In our case this corresponds to about $128^2 \simeq 16\,000$ gridpoints, a grid which we have found to give numerically accurate results for the systems considered in this work.

4 Variational quantum Monte Carlo

For comparison, a set of variational quantum Monte Carlo [31] (VMC) calculations were performed. In a VMC study, some initial guess must be invented for the wave function. This trial wave function has free adjustable parameters, $\Psi = \Psi(\{\alpha_i\})$, which are optimized to minimize the total energy. In the case of a single parabolic quantum dot, high symmetry fixes the single-particle part of the wave function, and free parameters adjust the electron-electron correlation part only.

In this study, the minimization process of variational parameters was performed using stochastic gradient approximation [32], which is tailored to minimize a function whose values are superimposed by statistical noise. The speed of the procedure can be greatly increased by using analytic expressions for certain derivatives [33], and as a result a single VMC run with full two-parameter minimization and calculation of selected observables is a matter of a few minutes on a regular workstation.

5 Single six-electron dot

The CSDFT and SDFT methods are used to calculate the electronic structure of a six-electron parabolic quantum dot in GaAs. In the calculations we have chosen the confining potential to be parabolic

$$V_{\rm ext}(\mathbf{r}) = \frac{1}{2}m^*\omega_0^2 r^2, \quad (12)$$

where $\hbar\omega_0$ is the confinement strength. There are mainly two reasons which make this system particularly interesting. First of all, it corresponds to the smallest dot size

for which there are two classically stable crystalline structures: a pentagonal ring with one electron at the centre (the (5,1) electron configuration), and a sixfold ring (the (6,0) electron configuration) [35]. Secondly, it corresponds to a magic configuration of a 2D harmonic well. In other words, the energy shells are fully closed and the Fermi gap is particularly large.

5.1 Zero magnetic field and the weak confinement limit

At first we omit the magnetic field and examine the system as the confinement strength $\hbar\omega_0$ is lowered. In Figure 1 we show our SDFT results for the energy difference between the paramagnetic ($S_z = 0$) and the polarized ($S_z = 3$) spin states as a function of the confining potential. The results are compared with those obtained by the VMC by three of the present authors in a previous work [13]. In the SDFT calculations the confinement can be set to 0.1 meV without problems in the convergence. The energy difference is clearly greater in the SDFT results than in the VMC ones. However, one should bear in mind that the values are differences between total energies which are of the order of two or three decades larger in magnitude. At low confinement both the methods give the spin-polarized state as the ground state. According to the VMC the transition occurs at about 0.28 meV whereas in the SDFT the confinement has to be lowered to about 0.18 meV before the polarization takes place.

The next object of interest is the spontaneous symmetry breaking of the spin densities. The concept of spin density waves (SDW) was first introduced by Overhauser [36], who proved that the Hartree-Fock ground state of the homogenous electron gas at low electron densities is not the usual paramagnetic state. Instead it is possible to construct a spin density wave with a lower total energy. This energy difference arises from the lowering of the exchange energy which is only partially compensated by the rise of the kinetic energy, leading to a static SDW.

Our SDFT calculations give for the six-electron dot the SDW behavior as the confinement is lowered below $\hbar\omega_0 \approx 0.45$ meV. Figures 2 and 3 show the gradual development. Above the transition point the total electron density of the $S_z = 0$ ground state has a (6,0)-like electron configuration, *i.e.* there is a minimum of the density in the centre and a maximum at a finite radius, as depicted in Figure 2 for $\hbar\omega_0 = 0.6$ meV. The polarized state, $S_z = 3$, corresponding to the first excited state, has a (5,1)-like configuration, *i.e.* the electron density has a maximum in the centre and a less pronounced maximum at the dot radius. When the confinement is lowered, the relative amplitude of the SDW grows rapidly as shown in the top row of Figure 3 for the spin density. Actually, the maximum value of the (spin) density grows at the beginning of the localization in spite of the weakening confinement. The spin-up and spin-down densities are symmetrically coupled with each other resulting in a SDW-like polarization, and the ensuing total electron density shows localization around six maxima as depicted in the bottom graph of Figure 3.

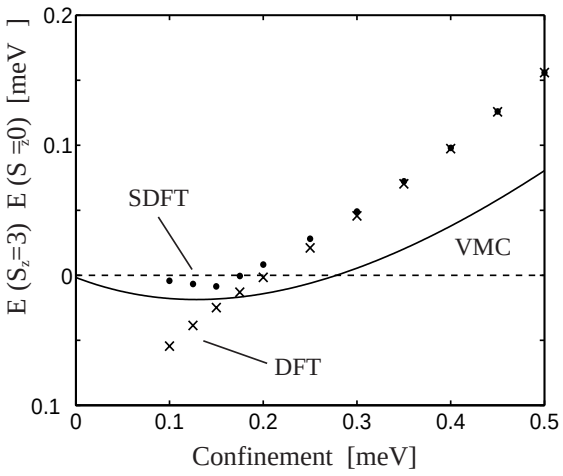

Fig. 1. Six-electron dot. The energy difference between the spin polarized $S_z = 3$ and the paramagnetic $S_z = 0$ spin states as a function of the confinement. The dots are the SDFT results, the solid line corresponds to the VMC results taken from reference [13]. The crosses mark the results of the spin-compensated DFT-LDA calculations.

We have studied in the SDFT the effects of the (simultaneous) spin and circular symmetry breaks on the total energy of the $S_z = 0$ state and on the energy difference between the $S_z = 3$ and $S_z = 0$ state. This is done by performing for the $S_z = 0$ state symmetry conserving DFT calculations within the LDA. Note that in our calculations for the $S_z = 3$ state the circular symmetry is conserved. The symmetry break in the $S_z = 0$ state lowers the total energy so that the difference between the symmetry breaking and the symmetry conserving solutions increases with decreasing confinement. The difference is rather small on the energy scale of Figure 1, for example for $\hbar\omega_0 = 0.41$ meV it is 0.016 meV. However, requiring the symmetry conservation leads to an important qualitative effect. Namely, that the energy difference between the $S_z = 3$ and $S_z = 0$ states does not show a minimum in the confinement range for which we have been able to obtain converged results, but the difference seems to increase toward to the zero confinement limit (Fig. 1). Thus, the symmetry breaking solution with spatial regions of specific spin densities describes better the low confinement limit than the symmetry-conserving solution in which the spin-up and spin-down densities compensate each others at every point.

It is interesting that after the symmetry break one can see in the total electron density a maximum at the centre of the dot (see the bottom graph of Fig. 3). It becomes even clearer as the confinement is still lowered. This unexpected behavior is due to the eigenstate structure consisting of a non-degenerate and doubly-degenerate states for each spin direction. The non-degenerate states have a maximum at the centre of the dot whereas the doubly-degenerate states give the main contributions to the six maxima at the radius of the dot. Below the confinement

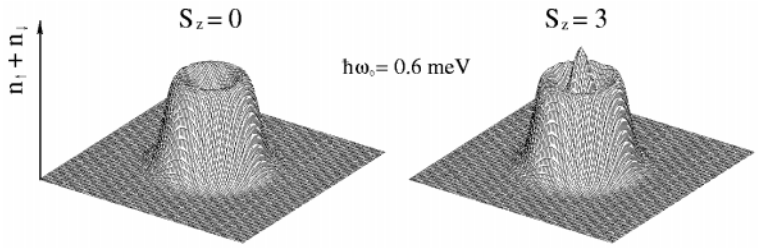

Fig. 2. Six-electron dot with $\hbar\omega_0 = 0.6$ meV. The total electron densities for the $S_z = 0$ and $S_z = 3$ spin states. The maximum amplitudes are 0.011 and 0.015 a_0^{*-2}, respectively. The side length of the region is 64 a_0^*.

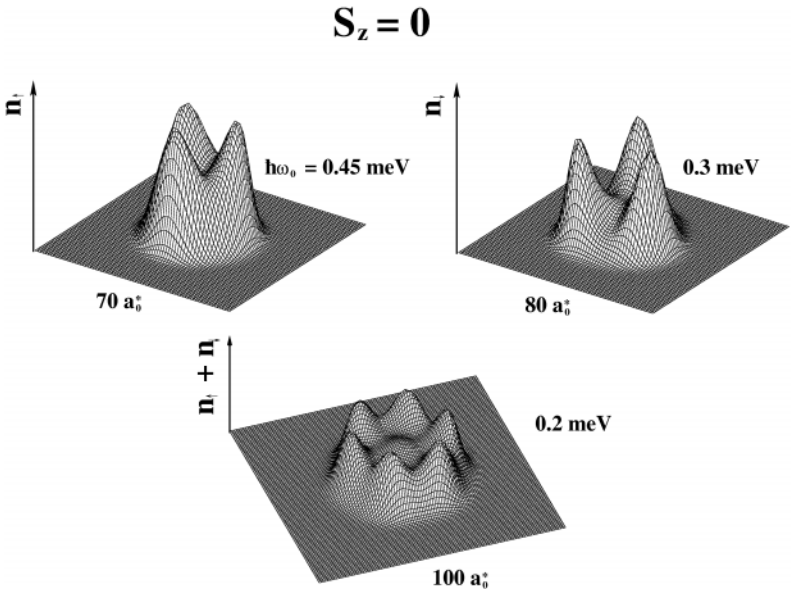

Fig. 3. Six-electron dot in the $S_z = 0$ state. The top row gives the spin densities for $\hbar\omega_0 = 0.45$ and 0.3 meV. The maximum values are 0.005, and 0.0044 a_0^{*-2}, respectively. The bottom graph gives the the total electron density for $\hbar\omega_0 = 0.2$ meV. The maximum value is 0.0038 a_0^{*-2}. The side lengths of the regions shown are 70 and 80 a_0^* for the confinements of 0.45 meV and 0.3 meV, respectively, and 100 a_0^* in the bottom graph.

of $\hbar\omega_0 = 0.18$ meV the $S_z = 3$ state is the ground state with a (5,1)-type electron density similar to that shown in Figure 2. One would expect the electrons to localize around their classical positions, namely in a pentagonal ring, as the electron density is lowered, and form a Wigner molecule. However, SDFT leads to difficulties at the low density limit as the correlation effects begin to dominate.

Spin density waves arising from SDFT calculations were observed in quantum dots by Koskinen *et al.* [19]. They found that static spin density waves can occur at low densities of the electron gas. In the case of filled shell QD's the onset of the SDW-like state was obtained at relatively low confinement, *e.g.*, at $\hbar\omega_0 < 0.7$ meV for a six-electron dot in agreement with our results. For larger dots, *e.g.*, for $N = 24$ or 34, they found that the SDW state with $S_z = 0$ becomes even lower in energy than the states obeying the Hund rule. Their results have been criticized by Hirose and Wingreen [21], who found the same breaking of Hund's rule but concluded that the SDW states are artifacts of broken spin symmetry in density-functional theory.

The classical crystallization of a six-electron parabolic quantum dot has been studied by unrestricted Hartree Fock (HF) calculations [12]. In these calculations the paramagnetic state, $S_z = 0$, was shown, in contrast with our SDFT results, to depict a crossover from a (6,0) arrangement to a (5,1) geometry at $\hbar\omega_0 \approx 1.5$ meV. Reimann *et al.* [11] found by configuration interaction calculations that the true ground state is unpolarized with the (6,0) symmetry if $\hbar\omega_0 > 1$ meV. This supports the results by Egger *et al.* [10] obtained by path integral Monte Carlo simulations. In the previous VMC calculations [13] the system spin-polarizes below $\hbar\omega_0 \approx 0.28$ meV, and when the confinement strength is reduced further the electrons begin to localize to the classical (5,1) configuration. The total energies of the $S_z = 0$ and $S_z = 3$ spin states obtained by exact diagonalization [11] agree with the VMC results of Figure 1 for confinements $\hbar\omega_0 > 0.3$ meV. However, the exact diagonalizations of Reimann *et al.* were limited to $\hbar\omega_0 > 0.3$ meV, and they could not reach the regime where the VMC results show spin polarization. Reimann *et al.* [11] also performed SDFT calculations, the results of which are in a good agreement with the present ones for confinements $\hbar\omega_0 > 0.3$ meV. However, they do not consider weaker confinements where the spin polarized $S_z = 3$ state is lower in energy than the paramagnetic $S_z = 0$ state. This confinement region is numerically demanding and the results may depend on the type of numerical solution of the SDFT problem.

Reimann *et al.* use the plane wave expansion in contrast to our real-space approach. The unrestricted HF calculations by Yannouleas and Landman [22] show spin polarization, spontaneous symmetry breaking and electron localization already when the confinement has decreased to the value of $\hbar\omega_0 \approx 1.1$ meV. This value is in clear disagreement with the VMC result of 0.28 meV. The SDFT predicting the transition at 0.18 meV seems to be an improvement over the unrestricted HF.

5.2 Uniform magnetic field

We have studied the effect of an external uniform magnetic field on the electronic structure of the $N = 6$ quantum dot using the CSDFT, SDFT and VMC methods. The magnetic field is applied perpendicular to the plane of 2D electron gas (in the direction of the z-axis). The confinement strength is chosen to be $\hbar\omega_0 = 5$ meV. This is a weak potential compared to real atomic systems and makes the correlation phenomena in the system relatively important. The magnetic length ($l_B = \sqrt{\hbar/eB} \approx 26$ nm at $B = 1$ T) is also comparable to the dot dimension (about 50 nm) causing transitions as the magnitude of the field is changed.

In the VMC calculation, two different methods are used to construct the many-body wave function. The method used in higher fields (beyond the maximum-density droplet) is explained in reference [37], and in lower fields, the Slater-Jastrow form is used:

$$\Psi = D_\uparrow D_\downarrow J\,. \tag{13}$$

Here $D_{\uparrow(\downarrow)}$ is a Slater determinant for spin up (down) electrons, and J is a Jastrow factor responsible for correlations. The determinants are filled with Fock-Darwin single-particle states [38] in such a way that only compact many-body states are obtained. Compact states are defined as states that have no gaps in occupation numbers $n_L = (n + l)/2$ and $n_I = (n - l)/2$, where n is the shell index and l is angular momentum quantum number [39].

The Jastrow factor J is a pair correlation function, and of the form:

$$J(\mathbf{R}) = \prod_{i<j} \exp\left(\frac{b_{ij} r_{ij}}{1 + a_{ij} r_{ij}}\right), \tag{14}$$

where b_{ij}'s are determined by cusp conditions, and a_{ij} are variational parameters. Only two different parameters were used, $a_{\uparrow\uparrow}$ for parallel-spin electron pairs, and $a_{\uparrow\downarrow}$ for antiparallel pairs. These parameters were optimized separately for each magnetic field and total spin value. In similar studies [40] this form of the Jastrow factor has been shown to be able to capture almost all of the correlation energy of small systems.

In the CSDFT and SDFT calculations we find that even if the external potential is circularly symmetric the internal effective potential V_σ can be nonsymmetric and break the spin symmetry. This is due to the localization of the electrons to different regions in space. The localization increases the kinetic energy but in favorable cases this effect is smaller than the lowering of the exchange-correlation energy. If the state is not circularly symmetric the wavefunctions are not pure eigenstates of the L_z operator. Therefore the broken circular symmetry is seen from the calculated L_z as a non-integer number.

The ground state energies corresponding to the CSDFT, SDFT, and VMC calculations and different values for the total S_z are shown in Figure 4 as functions of the external field. In the $S_z = 0$ case, the CSDFT calculations were done also by forcing the spin densities to be equal and thereby to preserve the spin symmetry. The scheme is analogous to the DFT-LDA and it is therefore denoted as the CSDFT-LDA. Up to the medium fields of 4 T the different schemes give rather consistent energy values for the $S_z = 0$, $S_z = 1$ and $S_z = 2$ configurations. In the high fields the CSDFT gives energies which are lower than those obtained with the VMC for the $S_z = 0$ configuration. Much of this effect is due to the broken symmetry lowering the total energy of the system. This can be seen from Figure 4a where the forced spin symmetry of the CSDFT-LDA calculations brings the results closer to the VMC ones. The L_z values obtained from the CSDFT calculations are also given in Figure 4 so that the magnetic field values at which L_z changes are indicated by arrows. The regions of non-integer L_z, denoted by SB, indicate broken circular symmetry. In these regions L_z increases gradually starting from the value of the previous region. It should be noted that the minimum energy state is always circularly symmetric.

The minimum energy over all (circularly symmetric) configurations is plotted in Figure 5. The overall agreement between the CSDFT and VMC results is good. It is striking that for the $L_z = 6$, $S_z = 0$ and $L_z = 15$, $S_z = 3$ regions the methods give results in an astonishing agreement. The latter region is the MDD domain in which all the adjacent single-electron states from $L_z = 0$ to $L_z = 5$ are occupied with one spin-up electron resulting in a totally spin-polarized system. Similarly in the $L_z = 6$, $S_z = 0$ domain all the adjacent single-electron states from $L_z = 0$ to $L_z = 2$ are occupied with two electrons resulting in a spin-compensated system, which is a MDD for both spin-up and spin-down electrons. These two regions are characterized with compact electron densities which are rather flat in the interior of the quantum dot. In the region where the minimum energy configuration is $L_z = 10$, $S_z = 2$ the CSDFT, SDFT and VMC results differ more from each other. Thus we can conclude that the exchange-correlation functionals are surprisingly accurate for the two limits, the spin-compensated and the spin-polarized electron gas but there are more problems in constructing an exchange-correlation functional for partial spin polarizations. The methods give consistent B values for the transition points. However, in the SDFT and in the VMC a transition occurs at ≈ 4.0 T to a state with $L_z = 7$, $S_z = 1$ which is absent in the CSDFT. The reason for the difference is that the energies of the $L_z = 10$, $S_z = 2$ states are about 0.5 meV lower in energy than the corresponding states in the VMC and in the SDFT.

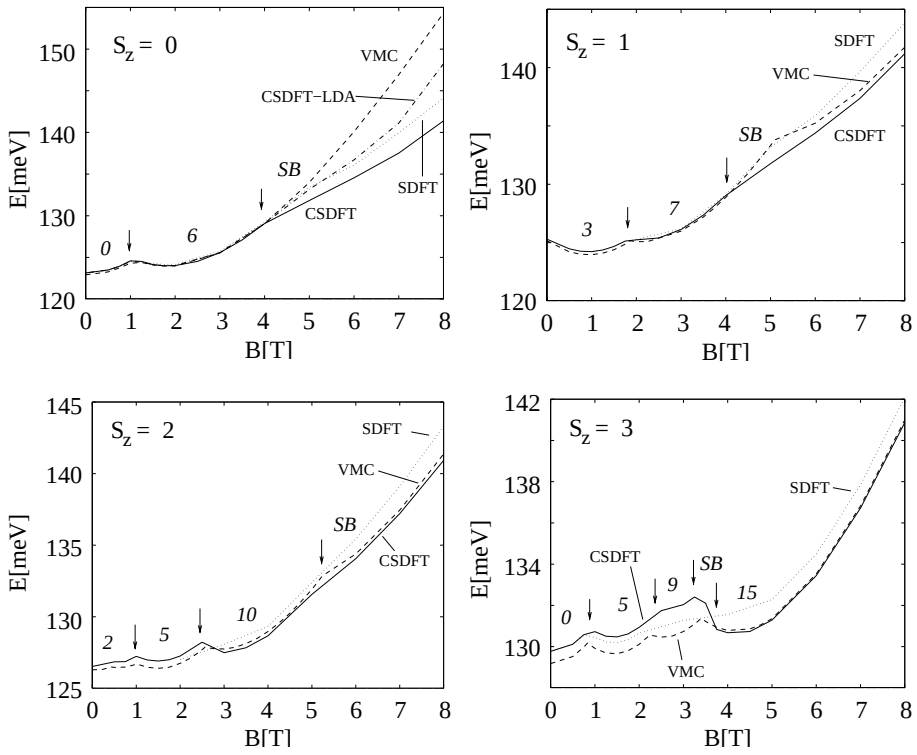

Fig. 4. Six-electron quantum dot $\hbar\omega_0 = 5$ meV. Total energy as a function of the magnetic field for the different S_z values. The solid line is the CSDFT energy, the dashed line is the VMC energy and the dotted line is the SDFT energy. The dash-dotted line in the graph (a) corresponds to the CSDFT-LDA calculations using spin-compensation, *i.e.* forcing the spin-up and spin-down densities to be equal. The arrows denote the transition points in the CSDFT results between the different $(-L_z)$ states given by italic numbers. SB means the broken circular symmetry and a non-integer (L_z) value. In the case $S_z = 0$ the VMC result in high B is significantly higher than in other calculations. This is due to the restriction of using only compact states in the VMC study.

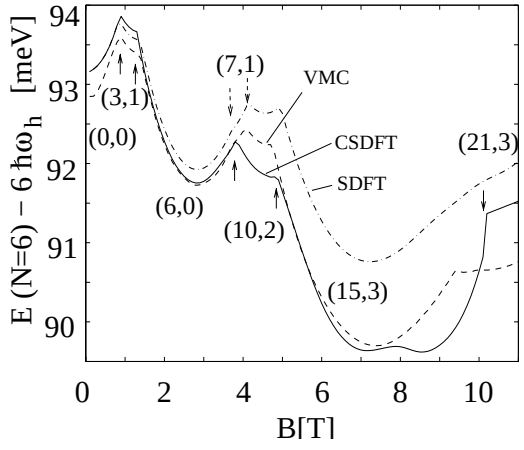

Fig. 5. Six-electron quantum dot $\hbar\omega_0 = 5$ meV. Ground state energy (minus 6 $\hbar\omega_h = 6\,\hbar\sqrt{\omega_0^2 + (\omega_c/2)^2}$, where $\omega_c = eB/m^*$ is the cyclotron frequency) as a function of magnetic field. The solid line is the CSDFT result, the dashed line is the VMC energy and the dash-dotted line is the SDFT energy. The transition points between the $(-L_z, S_z)$ states in the CSDFT results are marked with arrows. In the VMC and CSDFT results there is one more transition at ≈ 3.8 T to the state with $L_z = -7$, $S_z = 1$ (left dashed arrow). In both schemes this state changes to the $L_z = 10$, $S_z = 2$ at ≈ 4.1 T (right dashed arrow).

The differences reflect again difficulties in constructing an exchange-correlation functional of general validity.

In the CSDFT and in the SDFT there is a transition from the MDD state to the $L_z = 21$, $S_z = 3$ state at $B \approx 10\ T$. The corresponding VMC transition occurs at $B \approx 9\ T$. In this beyond-MDD region we find that it is difficult to get converged results with the CSDFT method. The problem is less severe with the SDFT than the CSDFT, since in the former the self-consistency condition includes only the scalar potential whereas in the latter also the exchange-correlation vector potential has to be solved self-consistently. Due to poor convergence we omit the excited $S_z = 2$, $S_z = 1$ and $S_z = 0$ states from the CSDFT results in this domain. The CSDFT $S_z = 3$ states converge to a good accuracy up to the field strength of $B = 11\ T$ by applying a finite temperature to the system. This shifts the total energy curve to the right by about 1.0 T (Fig. 5).

6 Double dot

Finally, we consider the system of two laterally coupled quantum dots at the interface of the GaAs/AlGaAs heterostructure. The dots contain one electron each, so that the system is reminiscent of the hydrogen molecule. The dots are considered to be located near each other which

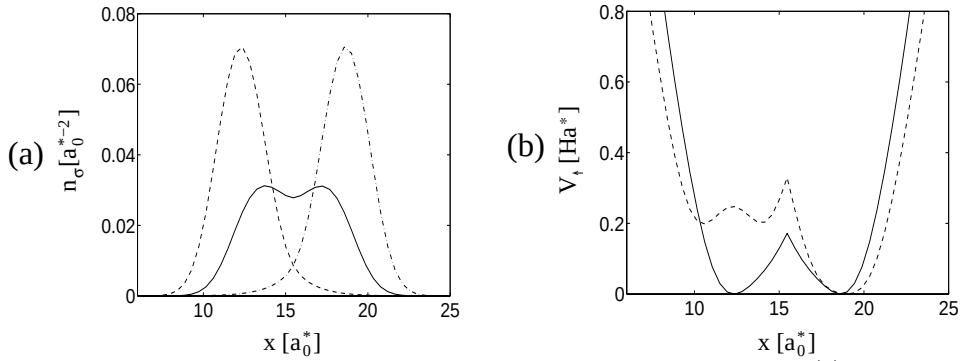

Fig. 6. Two-electron double dot. The confinement strengths of the dots are $\hbar\omega_0 = 3$ meV. (a) Spin densities along the axis joining the dot centra for the inter-dot separations of 3 a_0^* (solid curve) and 6 a_0^* (The dashed curve is the spin up-density and the dash-dotted curve is the spin-down density). (b) The corresponding effective potentials for the inter-dot separations of 3 a_0^* (solid curve) and 6 a_0^* (dashed curve. Only the spin-up potential is shown. The spin-down potential is a mirror image of the spin-up potential).

allows the tunneling of electrons between the dots. An external magnetic field perpendicular to the plane of the 2D electron gas is applied. We calculate the electronic structure of this system using the CSDFT and the VMC.

In the calculations for the magnetic field response of this double dot system we have chosen the external potential to be a quartic polynomial [18]

$$V(x,y) = \frac{m^*\omega_0^2}{2}\left[\frac{1}{4a^2}(x^2-a^2)^2 + y^2\right], \qquad (15)$$

where the centra of the dots are at $x = \pm a$. The interdot distance $d = 2a$. Near the dot centra the polynomial separates into two harmonic wells with the confinement $\hbar\omega_0$. Between the dots there is a potential barrier of the height of $V = 1/8m^*\omega_0^2 a^2$. In order to compare the results to those by Wensauer *et al.* [17] we have also used in the zero-B-field case the model potential

$$V(\mathbf{r}) = \frac{1}{2}m^*\omega_0^2 \min\left[(\mathbf{r}-\mathbf{a})^2, (\mathbf{r}+\mathbf{a})^2\right]. \qquad (16)$$

In our calculations we have chosen $\hbar\omega_0$ to be 3 meV. The Hamiltonian of the system is the same as in equation (1) and the Kohn-Sham equations in the CSDFT are given in the Section 2.2.

We have performed unrestricted CSDFT calculations and allowed the spin density to break the symmetry of the problem by localizing the electrons if it lowers the total energy. Thus, in the present system the broken symmetry means that in the $S_z = 0$ total spin state the effective potential for the spin up electron has the global minimum at one of the two dot centra whereas there is only a local minimum at the adjacent dot centre. For the spin down electron the dots have changed their roles. This is shown in Figure 6 for the double dot in zero magnetic field. The symmetry breaking is again due to the lowering of the exchange-correlation energy in LSDA as the spin polarization increases. This energy lowering overcomes the increase in the kinetic energy due to the localization. The symmetry of the wavefunctions can be preserved by using the spin-compensated LDA instead of the LSDA.

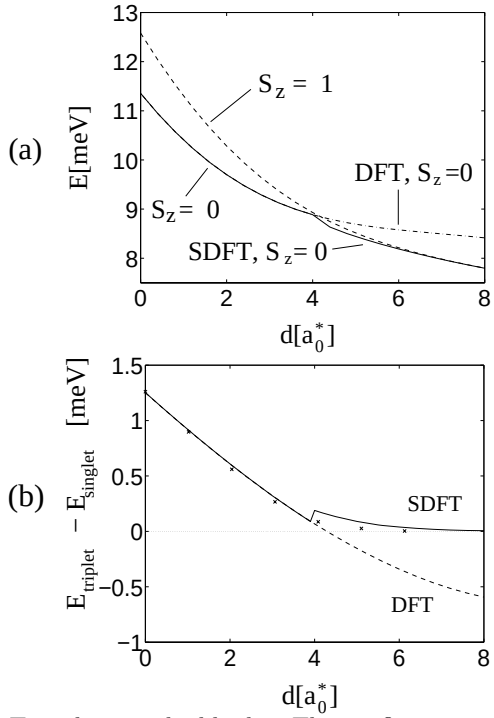

Fig. 7. Two-electron double dot. The confinement strengths of the dots are $\hbar\omega_0 = 3$ meV. (a) Zero-B-field total energy as a function of the inter-dot separation d. The SDFT energies of the $S_z = 0$ and $S_z = 1$ states are given by the solid and dashed curves, respectively. The cusp in the SDFT energy curve is due to the transition to the symmetry-breaking solution. The energy corresponding to the symmetry-preserving DFT is shown as the dash-dotted curve. (b) The singlet-triplet energy separation as a function of inter-dot distance. The SDFT and the VMC results are denoted by the solid curve and the ×-marks, respectively. The discontinuity in the SDFT energy curve is due to the transition to the symmetry breaking solution. The energy separation corresponding to the symmetry-preserving DFT is shown as the dashed curve.

In Figure 7 the zero-B-field SDFT and DFT total energies and the singlet-triplet separation are plotted as a function of the inter-dot distance. We let the $S_z = 0$ and $S_z = 1$ states of the SDFT or DFT calculations to represent the singlet and triplet states, respectively, although

in these theories we cannot define the total spin S of the two electrons. However, the fact that density-functional theories give the lowest energy states of each different spin symmetry should give credence to our identification. The results were calculated using equation (16) for the external potential. The density-functional $S_z = 0$ solution splits into symmetry breaking and symmetry conserving solutions above 4.5 a_0^*. The symmetry conserving solution is calculated with the spin-compensated DFT within the LDA. At large inter-dot distances the energy of the symmetry breaking $S_z = 0$ state and that of the $S_z = 1$ state approach each other. The total energy curve behaves as $1/d$ since the dots are well separated and the total energy is dominated by the Coulomb repulsion between the two dots. This is the regime where the tunneling probability of the electrons through the potential barrier $V = 1/8m^*\omega_0^2 a^2$ is negligible. There is a cusp in the energy curve at around $d = 4.5$ a_0^* where the transition to the localized states happens. The cusp is an indication that the LSDA is not a good approximation in this intermediate region but gives the correct behaviour away from this region. The symmetry-breaking SDFT results give the correct prediction that the singlet state is lower in energy than the triplet state, and reproduce also in the large-separation limit the equality of the singlet and triplet state energies. The qualitative behaviour of the DFT-LDA result is the same as that obtained by Wensauer *et al.* [17] who excluded the symmetry breaking solutions explicitly in their calculations.

The calculated singlet-triplet separation is compared with the variational Quantum Monte Carlo result in Figure 7b. To check the accuracy of the VMC, we have performed diffusion QMC simulations for the $S = 0$ state at various distances [41]. The lowering of the energy from the VMC to the diffusion quantum Monte Carlo is found to be small, only about 0.02 meV. At small distances the SDFT and VMC results are in a remarkable agreement, strengthening the conclusion that the exchange-correlation effects for the spin-compensated and totally spin-polarized gas are well described in the LSDA. The fact that after the symmetry break the SDFT results are above the VMC ones may reflect the fact that the symmetry breaking lowers the singlet-state energy too much in comparison to the symmetry-conserving VMC. In conclusion, the symmetry-unrestricted SDFT gives a better approximation for the ground state energy of the double dot molecule than the symmetry-conserving DFT. The symmetry conserving solution is unphysical at large inter-dot distances. Our conclusions are in accord with the results by Gunnarsson and Lundqvist who studied the dissociation of the H_2 molecule within the SDFT and the DFT [6].

We have calculated the magnetic field dependence of the $S_z = 0$ and $S_z = 1$ states for the double dot with the separation of $d = 2.73$ a_0^* up to the magnetic field strength of 6 T. The resulting singlet-triplet separation is plotted in Figure 8. The CSDFT predicts a transition from the singlet configuration to the triplet configuration at $B = 1.5$ T. The symmetry of the $S_z = 0$ solution of the CSDFT state is broken at $B = 2.2$ T. Thereafter the

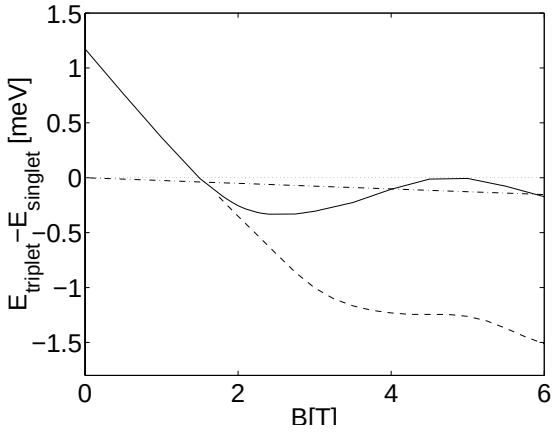

Fig. 8. Two-electron double dot. The inter-dot distance is 2.73 a_0^* and the confinement strengths of the dots are $\hbar\omega_0 = 3$ meV. The singlet-triplet separation (solid line) is given as a function of the external magnetic field B. The calculations were done using the CSDFT within the LSDA. The results corresponding to the symmetry-preserving, spin-compensated CSDFT-LDA are also shown (dashed line). The magnitude of the Zeeman term is also plotted (dash-dotted line).

separation shows a minimum at $B = 2.5$ T. After this point the Zeeman energy dominates the high energy behaviour of the singlet-triplet splitting. If the Zeeman term is ignored in the energy functionals the singlet state becomes the ground state again at $B \approx 4$ T, there is a maximum in the separation at $B = 4.7$ T, and finally the separation vanishes at the high field limit. Inclusion of the Zeeman term lowers the energy of the triplet state. In this case the separation vanishes at $B = 4.7$ T and at the high field limit the triplet becomes again the ground-state. The above picture is qualitatively consistent with the Heitler-London and Hund-Mulliken calculations [18]. A closer quantitative comparison is difficult due to the quite large scatter also between the Heitler-London and Hund-Mulliken results. However, on the basis of the good agreement between the CSDFT and VMC results before the symmetry breaking in Figure 8 and in the zero-field case with electron localization in Figure 7b, we believe that our CSDFT results should be even quantitatively reliable at low magnetic field strengths. Especially, this holds for the position of the transition from the singlet to triplet state. This transition is important, because it makes the quantum dot molecule a possible candidate for a qubit of future quantum computers.

We show in Figure 8 also the results of the CS-DFT calculations obtained by using the spin-compensated CSDFT-LDA preserving the symmetry of the electron configuration. This scheme does not show a minimum value for the singlet-triplet separation, but the high-field limit can be considered as a very rough lower-bound approximation for the minimum and can be compared, for example, with the Heitler-London and Hund-Mulliken results.

According to the theory by von Barth [42] the symmetry-breaking solution for a two-electron system such as the present double quantum dot corresponds to a mixed state arising from the Slater determinants of the states $S = 0, S_z = 0$ and $S = 1, S_z = 0$. The singlet-triplet separation can in this scheme be approximated by doubling the energy separation of the symmetry-breaking $S_z = 0$ and the $S_z = 1$ solutions. If this scheme is applied in the case of the double-dot in magnetic field the depth of the minimum doubled. The results of the von Barth scheme is thus in a better agreement with the Hund-Mulliken results than those of Figure 8. It is also interesting to note that applying symmetrisation to the unrestricted HF results for a two-electron double dot approximately doubles the singlet-triplet separation [14]. However, the fact that doubling the singlet-triplet separation in the symmetry-break regime in our zero-field results (Fig. 7) increases the discrepancy between SDFT and VMC, sheds a shadow on the generality of the von Barth scheme.

7 Summary and outlook

We have performed density-functional (CSDFT and SDFT) calculations for the six-electron quantum dot and for the H_2 quantum dot molecule. The calculations are based on a symmetry-unrestricted solution of the Kohn-Sham equations using a novel real-space method. The results are compared with those arising from VMC calculations, performed in this work or published earlier.

We can conclude that the exchange-correlation effects are rather well taken into account in the density-functional schemes: (i) At the limit of the vanishing confinement in the zero magnetic field the SDFT and VMC total energies are in agreement, predicting a phase transition from the paramagnetic state to the totally spin-polarized state. In this region the SDFT shows the breaking of the spin symmetry and the circular symmetry of the electron density. (ii) The CSDFT predicts for the six-electron quantum dot the transitions between different angular momentum and spin states as a function of the external magnetic field in agreement with the VMC. The CSDFT is, as expected, more accurate in the high field limit than the SDFT since the effect of currents are ignored in the SDFT exchange-correlation functional. (iii) At small interdot distances the SDFT results for the singlet-triplet energy separation of the H_2 quantum dot molecule in zero magnetic field are in a quantitative agreement with those obtained by the VMC method. At large interdot distances the spin symmetry is broken in the SDFT. The singlet-triplet energy separation predicted by the SDFT and the VMC are in a qualitative agreement in this regime. As a function of the external magnetic field the CSDFT, allowing the spin symmetry to be broken, gives the correct qualitative behaviour in comparison with other theoretical models.

The agreement between the density-functional and the VMC results is especially good for spin-compensated and totally spin-polarized electron systems. This is true for the regime of finite magnetic field with the CSDFT as well as for the zero magnetic field when the CSDFT reduces to the SDFT. The success of the CSDFT in obtaining correct results depends, however, on the chosen approximations for the exchange and correlation functionals. Search for a correct parametrization of the LSDA functionals and approximations beyond the LSDA in the CSDFT should therefore be important for the future improvements in the electronic structure calculations of quantum dots.

This work has been supported by Academy of Finland through the Centre of Excellence Program (2000-2005). We thank M. Manninen and J. Kolehmainen for providing valuable information and data of the plane-wave solving methods of the CSDFT, M. Heiskanen and T. Torsti for sharing their experience on the Rayleigh quotient multigrid method, and J. von Boehm for valuable discussions.

References

1. P. McEuen, Science **5**, 1729 (1997).
2. A.O. Orlov, I. Amlani, G.H. Bernstein, C.S. Lent, G.L. Snider, Science **277**, 928 (1997).
3. D. Loss, D.P. DiVincenzo, Phys. Rev. A **57**, 120 (1998).
4. P. Hohenberg, W. Kohn, Phys. Rev. **136**, B846 (1964).
5. W. Kohn, L.J. Sham, Phys. Rev. **140**, A1133 (1965).
6. O. Gunnarsson, B.I. Lundqvist, Phys. Rev. B **13**, 4274 (1976).
7. G. Vignale, M. Rasolt, Phys. Rev. B **37**, 10 685 (1988).
8. We use the variational quantum Monte Carlo scheme by A. Harju, B. Barbiellini, S. Siljamäki, R.M. Nieminen, G. Ortiz, Phys. Rev. Lett. **79**, 1173 (1997).
9. See, for example, Ll. Serra, M. Barranco, A. Emperador, M. Pi, E. Lipparini, Phys. Rev. B **59**, 15 290 (1999).
10. R. Egger, W. Häusler, C.H. Mak, H. Grabert, Phys. Rev. Lett. **82**, 3320 (1999).
11. S.M. Reimann, M. Koskinen, M. Manninen, Phys. Rev. B **62**, 8108 (2000).
12. B. Reusch, W. Häusler, H. Grabert, Phys. Rev. B **62**, 113313 (2001).
13. A. Harju, S. Siljamäki, R.M. Nieminen, Phys. Rev. B **65**, 075309 (2002).
14. C. Yannouleas, U. Landman, Eur. Phys. J. D **16**, 373 (2001), `cond-mat/0107014`.
15. O. Steffens, U. Rössler, M. Suhrke, Europhys. Lett. **42**, 529 (1998).
16. A. Harju, V.A. Sverdlov, R.M. Nieminen, V. Halonen, Phys. Rev. B **59**, 5622 (1999).
17. A. Wensauer, O. Steffens, M. Suhrke, Ulrich Rössler, Phys. Rev. B **62**, 2605 (2000).
18. G. Burkard, D. Loss, D.P. DiVincenzo, Phys. Rev. B **59**, 2070 (1999).
19. M. Koskinen, M. Manninen, S.M. Reimann, Phys. Rev. Lett. **79**, 1389 (1997).
20. S.M. Reimann, M. Koskinen, M. Manninen, B.R. Mottelson, Phys. Rev. Lett. **83**, 3270 (1999).
21. K. Hirose, N.S. Wingreen, Phys. Rev. B **59**, 4604 (1999).
22. C. Yannouleas, U. Landman, Phys. Rev. Lett. **82**, 5325 (1999).

23. M. Koskinen, M. Manninen, B. Mottelson, S.M. Reimann, Phys. Rev. B **63**, 205323 (2001).
24. M. Heiskanen, T. Torsti, M.J. Puska, R.M. Nieminen, Phys. Rev. B **63**, 245106 (2001).
25. C. Weisbuch, C. Hermann, Phys. Rev. B **15**, 816 (1977), http://link.aps.org/abstract/PRB/v15/p816.
26. B. Tanatar, D.M. Ceperley, Phys. Rev. B **39**, 5005 (1989).
27. D. Levesque, J.J. Weis, A.H. MacDonald, Phys. Rev. B **30**, 1056 (1984).
28. M. Ferconi, G. Vignale, Phys. Rev. B **50**, 14 722 (1994).
29. M. Koskinen, J. Kolehmainen, S.M. Reimann, J. Toivanen, M. Manninen, Eur. J. Phys. D **9**, 487 (1999).
30. J. Mandel, S. McCormick, J. Comput. Phys. **80**, 442 (1989).
31. W.M.C. Foulkes, L. Mitas, R.J. Needs, G. Rajagopal Rev. Mod. Phys. **73**, 33 (2001).
32. A. Harju, B. Barbiellini, S. Siljamäki, R.M. Nieminen, G. Ortiz, Phys. Rev. Lett. **79**, 1173 (1997).
33. X. Lin, H. Zhang, A.M. Rappe, J. Chem. Phys. **112**, 2650 (2000).
34. O. Steffens, Michael Suhrke, Phys. Rev. Lett. **82**, 3891 (1999).
35. F. Bolton, U. Rössler, Superlattices Microstruct. **13**, 139 (1992); V.M. Bedanov, F.M. Peeters, Phys. Rev. B **49**, 2667 (1994).
36. A.W. Overhauser, Phys. Rev. **128**, 1437 (1962).
37. S. Siljamäki, A. Harju, R.M. Nieminen, V.A. Sverdlov, P. Hyvönen, Phys. Rev. B **65**, 121306(R) (2002), cond-mat/0112243.
38. V. Fock, Z. Phys. **47**, 446 (1928).
39. Our definition of compact states is more restrictive than the one given in J.K. Jain, T. Kawamura, Europhys. Lett. **29**, 321 (1995).
40. A. Harju, V.A. Sverdlov, R.M. Nieminen, Europhys. Lett. **41**, 407 (1998).
41. A. Harju, S. Siljamäki, R.M. Nieminen, unpublished.
42. U. von Barth, Phys. Rev. A **20**, 1693 (1979).
43. A. Harju, S. Siljamäki, R.M. Nieminen, Phys. Rev. B **60**, 1807 (1999).